Harmonic Analysis of DC-Link Capacitor Current in Sinusoidally Modulated Neutral-Point-Clamped Inverter

K.S. Gopalakrishnan and G. Narayanan

***Abstract*—The voltage ripple and power loss in the DC-capacitor of a voltage source inverter depend on the harmonic currents flowing through the capacitor. This paper presents double Fourier series based harmonic analysis of DC capacitor current in a three-level neutral point clamped inverter, modulated with sine-triangle PWM. The analytical results are validated experimentally on a 5-kVA three-level inverter prototype. The results of the analysis are used for predicting the power loss in the DC capacitor.**

***Index Terms*—Capacitor current, capacitor loss, diode-clamped inverter, double Fourier series, harmonic analysis, neutral-point-clamped inverter, three-level inverter.**

I. Introduction

THREE-level neutral-point clamped inverter is being used widely these days [1] [2]. The harmonic spectrum of the output voltage has been studied extensively for both two-level [3][4] and three-level inverters [3][5]. Harmonic analysis of the DC-capacitor current in a two-level inverter based on double Fourier series and geometric wall model [3] is presented in [6]. A brief description on the utilisation of this technique for determination of harmonic spectrum of DC-link current for three-level diode-clamped inverter is given in [7].

This paper presents a detailed discussion on the application of the above techniques for the harmonic analysis of DC-link current in a three-level inverter. The analytical results are validated extensively through experimental results. Further, the results of the harmonic analysis are used to evaluate the power loss in DC capacitors.

The DC-link current in a diode-clamped inverter is expressed mathematically in terms of load current and device switching state in section II. Harmonic analysis of the DC-link current based on double Fourier series and geometric wall model techniques is presented in section III. The results of the analysis are validated experimentally on a 5-kVA NPC inverter. The analytical and experimental results are compared in section IV. The power loss in the DC capacitor is estimated using the above harmonic analysis and the equivalent series resistance (ESR) of the capacitor at different operating conditions in section V. The conclusions are presented in section VI.

K.S.Gopalakrishnan is with the Department of Electrical Engineering, Indian Institute of Science, Bangalore - 560012, (ashwinkrishnan121@gmail.com)

G.Narayanan is with the Department of Electrical Engineering, Indian Institute of Science, Bangalore - 560012, (gnar@ee.iisc.ernet.in)

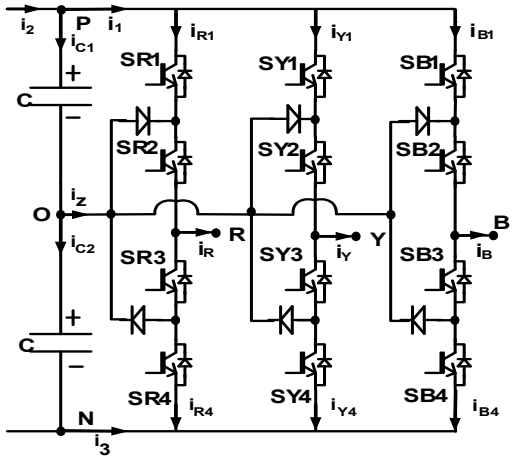

Fig. 1. Three-level neutral-point-clamped inverter

II. DC-Link Current in an NPC Inverter for In-Phase SPWM Scheme

The power circuit of a three-level neutral-point-clamped inverter is shown in Fig.1. The three legs are switched by comparing three-phase sinusoidal modulating signals against two level-shifted, in-phase, triangular carriers as illustrated in Fig.2. The R-phase modulating wave $f(\omega t)$, the top carrier wave $g_1(\omega_c t)$, and the bottom carrier wave $g_2(\omega_c t)$ are described mathematically in (1), where *M* is the modulation index; ω_c is the carrier angular frequency; ω is the fundamental angular frequency.

$$\begin{aligned} f(\omega t) &= M sin(\omega t) && \frac{-\pi}{2} < \omega t < \frac{3\pi}{2} \\ g_1(\omega_c t) &= -\omega_c t/\pi && -\pi < \omega_c t < 0 \\ g_1(\omega_c t) &= \omega_c t/\pi && 0 < \omega_c t < \pi \\ g_2(\omega_c t) &= -1 - \omega_c t/\pi && -\pi < \omega_c t < 0 \\ g_2(\omega_c t) &= -1 + \omega_c t/\pi && 0 < \omega_c t < \pi \end{aligned} \tag{1}$$

The harmonic content of the line current in a sinusoidally modulated NPC inverter is quite low [3], [5]. Since these line current harmonics are insignificant to influence the DC-link current [6], the three-phase load currents i_R, i_Y and i_B can be expressed as shown in (2), where I_M is the peak fundamental

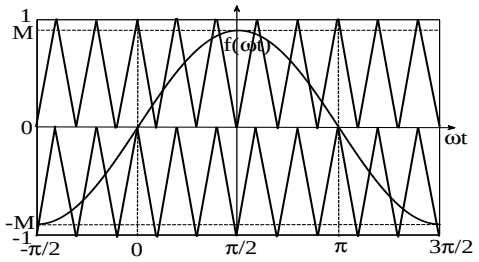

Fig. 2. Modulating signal $f(\omega t)$

current, and ϕ is the load power factor angle.

$$\begin{aligned} i_R &= I_M sin(\omega t - \phi) \\ i_Y &= I_M sin(\omega t - \frac{2\pi}{3} - \phi) \\ i_B &= I_M sin(\omega t + \frac{2\pi}{3} - \phi) \end{aligned} \tag{2}$$

The load current (say i_R) flows through the top switch (say SR1), whenever the switch is ON, i.e. when the modulation signal is greater than both the carriers. This is illustrated in Fig.3a, which considers a switching cycle corresponding to *M*=0.9, ωt=52°, and $f(\omega t) = 0.707$. The top-switch current (i_{R1}) is zero otherwise as shown by Fig.3a and Fig.3b; Fig.3b considers a switching cycle in the negative half cycle of $f(\omega t)$, i.e. *M*=0.9, $\omega t = -20°$ and $f(\omega t) = -0.3$. These conditions are expressed mathematically as shown in Table I.

i_{R1}	When $-\pi \leq \omega_c t \leq 0$	When $0 < \omega_c t \leq \pi$
i_R	$Msin(\omega t) > \frac{-\omega_c t}{\pi}$	$Msin(\omega t) > \frac{\omega_c t}{\pi}$
0	$\frac{-\omega_c t}{\pi} > Msin(\omega t)$	$\frac{\omega_c t}{\pi} > Msin(\omega t)$ ¡

TABLE I
CONDITIONS FOR DETERMINING TOP-SWITCH CURRENT i_{R1} IN A SWITCHING CYCLE

The sum of the three top-switch currents (i_{R1}, i_{Y1} and i_{B1}) gives the DC-link current i_1 as shown by (3).

$$i_1 = i_{R1} + i_{Y1} + i_{B1} \tag{3}$$

The DC link current i_1 consists of DC and AC components. The DC component (i_2) flows from the DC source or the rectifier. The entire ac component (i.e. $i_1 - i_2$) is assumed to flow through the DC capacitor. Hence the harmonic components of the DC capacitor current (i_{C1}) are the same as those of the DC-link current (i_1). Further, the harmonic analysis of the DC-link current i_1 can be broken up into that of the top-switch currents i_{R1}, i_{Y1} and i_{B1}. Since these are symmetric, the harmonic analysis of one of them (say i_{R1}) would suffice.

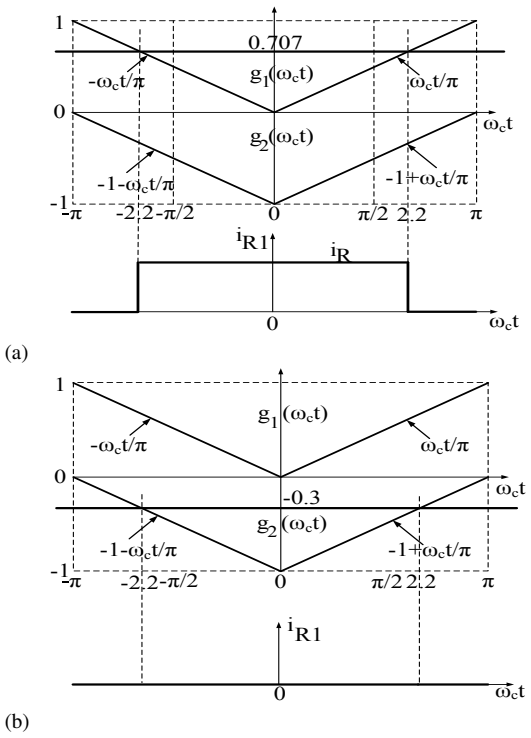

Fig. 3. Top switch current i_{R1} in a switching cycle when (a) M=0.9, ωt=52° and (b) M=0.9, ωt=−20°

III. HARMONIC ANALYSIS OF DC-CAPACITOR CURRENT

Harmonic analysis of the DC capacitor current i_{C1} reduces to that of the top-switch current i_{R1} as discussed above. The current i_{R1} depends on $f(\omega t)$, $g_1(\omega_c t)$ and $g_2(\omega_c t)$ which, in turn, depend on ωt and $\omega_c t$. Hence i_{R1} is a function of two independent variables ωt and $\omega_c t$. Further, it is periodic in both these variables. Hence i_{R1} is analysed based on double Fourier series [6] [3] in this paper.

A. Double Fourier Series Analysis

Fourier series is used for expressing periodic functions in one variable as summation of the DC, fundamental and harmonic components. Similarly, double Fourier series is used to express periodic functions in two variables, as summation of sinusoidal components whose frequencies can be represented as $m\omega_c + n\omega$, where *m* is a non-negative integer, and *n* is an integer. The integers *m* and *n* are called *carrier index* and *fundamental index*, respectively [3]. Any function $h(\omega t, \omega_c t)$, which is independently periodic in both ωt and $\omega_c t$, is expressed as given below [3].

$$\begin{aligned} h(\omega_c t, \omega t) = \frac{A_{00}}{2} &+ \sum_{n=1}^{\infty}[A_{0n}cos(n\omega t) + B_{0n}sin(n\omega t)] \\ &+ \sum_{m=1}^{\infty}[A_{m0}cos(m\omega_c t) + B_{m0}sin(m\omega_c t)] \\ + \sum_{m=1}^{\infty}\sum_{n=-\infty_{n\neq 0}}^{\infty} &[A_{mn}cos(m\omega_c t + n\omega t) + B_{mn}sin(m\omega_c t + n\omega t)] \end{aligned} \tag{4}$$

Where,

$$A_{mn} = \frac{1}{2\pi^2}\int_{-\pi/2}^{3\pi/2}\int_{-\pi}^{\pi} h(\omega_c t, \omega t)cos(m\omega_c t + n\omega t)d\omega_c t \;\; d\omega t$$
$$B_{mn} = \frac{1}{2\pi^2}\int_{-\pi/2}^{3\pi/2}\int_{-\pi}^{\pi} h(\omega_c t, \omega t)sin(m\omega_c t + n\omega t)d\omega_c t \;\; d\omega t \quad (5)$$

The complex form of A_{mn} and B_{mn} can be written as follows:

$$C_{mn} = A_{mn} + jB_{mn} = \frac{1}{2\pi^2}\int_{-\pi/2}^{3\pi/2}\int_{-\pi}^{\pi} h(\omega_c t, \omega t)e^{j(m\omega_c t + n\omega t)}d\omega_c t \;\; d\omega t \quad (6)$$

In equation (4), the first summation term, $\frac{A_{00}}{2}$, corresponds to the DC component of the waveform. The second summation term, $(\sum_{n=1}^{\infty}[A_{0n}cos(n\omega t) + B_{0n}sin(n\omega t)])$, corresponds to the fundamental and base-band harmonics. The third summation term, $(\sum_{m=1}^{\infty}[A_{m0}cos(m\omega_c t) + B_{m0}sin(m\omega_c t)])$, is the sum of carrier harmonics. The final summation term, $(\sum_{m=1}^{\infty}\sum_{n=-\infty_{n\neq 0}}^{\infty}[A_{mn}cos(m\omega_c t + n\omega t) + B_{mn}sin(m\omega_c t + n\omega t)])$, corresponds to the side-band harmonics [3].

B. Unit Cell

The top-switch current i_{R1} is a function in $\omega_c t$ and ωt as mentioned earlier. Hence it can be defined in a two-dimensional space with $\omega_c t$ and ωt as the orthogonal axes. Further, i_{R1} is periodic in both $\omega_c t$ and ωt. with a periodicity of 2π. Hence one needs to consider only an interval of 2π along each of the axes. Such a region bounded by one period of both variables is termed as *unit cell*. In this discussion, the unit cell is defined as the region formed by $-\pi < \omega_c t < \pi$ and $-\pi/2 < \omega t < 3\pi/2$ (see Fig.4a and Fig.4b).

C. Contour Plot

Double Fourier series and geometric wall modeling techniques have been widely used for harmonic analysis of PWM output waveforms of two-level and three-level inverters [3]. The PWM waveform has only discrete values (say high or low). Hence the unit cell can be divided into two (sets of) regions depending on the value of the waveform [3]. The boundary separating the two regions is termed as *contour plot*[3]. (More generally, the unit cell is divided into a number of regions, each corresponding to a particular value of the function). Such a method of analysis is called the 'geometric wall' method. This method is used for harmonic analysis of DC-link current in this work.

The top-switch current i_{R1} takes the values of i_R or zero. Hence the unit cell gets divided into two regions as discussed below.

Consider the switching cycle in Fig.3a. It can be represented by a vertical line AB (i.e. ωt=52°=0.903 rad) in the unit cell as shown in Fig.4a. The line segment PQ represents the duration for which $i_{R1} = i_R$ within this switching cycle. Further, the segments BQ and AP represent the intervals when $i_R = 0$ at the start and end of the switching cycle, respectively.

The switching cycle in Fig.3b, can be represented by a vertical line AB (i.e. ωt=-0.3 rad) in the unit cell shown in (4b). Since i_{R1}=0 in the entire duration of the sub cycle, the line segment PQ is of zero length as shown in Fig.4b. Both these points P and Q coincide with each other, and lie on the horizontal axis as shown in Fig.4b.

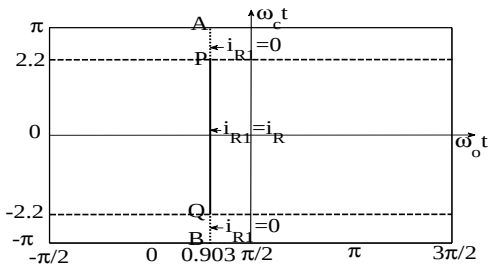

(a)

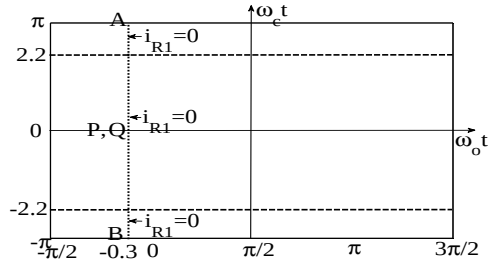

(b)

Fig. 4. (a) Representation of the switching cycle, $Fig.$3a in a unit cell (b) Representation of the switching cycle, $Fig.$3b in a unit cell

The loci of the points P and Q represent the boundary separating the regions where $i_{R1} = 0$ and $i_{R1} = i_R$. Therefore, the loci of the points P and Q yield the contour plot of i_{R1} shown in Fig.5. From Fig.5, it can be seen that the current $i_{R1} = i_R$ in the region between $\pi Msin(\omega t) < \omega_c t < -\pi Msin(\omega t)$. In all the other regions, $i_{R1} = 0$

D. Evaluation of Harmonic Components

The harmonic components of the current i_{R1} can be found by applying double Fourier integral on the function (i.e. i_{R1}) in the unit cell. This integral returns a zero value in all the regions except the region $-\pi Msin(\omega t) < \omega_c t < \pi Msin(\omega t)$, where the function assumes the value i_R. This reduced integral is given in (7). The harmonic components of currents i_{Y1}^{mn} and i_{B1}^{mn} are obtained from (7), by multiplying the same by $e^{2jn\pi/3}$ and $e^{-2jn\pi/3}$, respectively, as shown in (8) and (9).

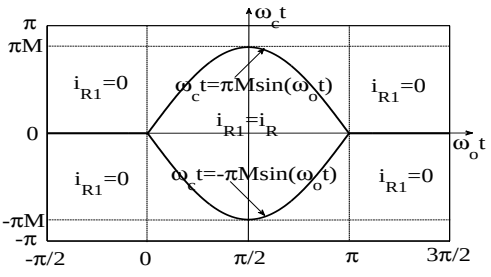

Fig. 5. Contour plot of i_{R1}

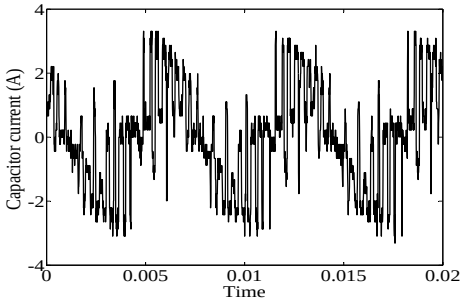

Fig. 6. Capacitor current waveform at I_M=4 A, modulation index of 0.9 at power factor of 0.844

$$i_{R1}^{mn} = \frac{1}{2\pi^2}\int_0^{\pi}\int_{-\pi Msin\omega t}^{\pi Msin\omega t} i_R e^{j(m\omega_c t+n\omega t)} d\omega_c t \;\; d\omega t \quad (7)$$

$$i_{Y1}^{mn} = \frac{1}{2\pi^2}\int_0^{\pi}\int_{-\pi Msin\omega t}^{\pi Msin\omega t} i_R e^{j(m\omega_c t+n\omega t)} d\omega_c t \;\; d\omega t \;\; e^{j(2n\pi/3)} \quad (8)$$

$$i_{B1}^{mn} = \frac{1}{2\pi^2}\int_0^{\pi}\int_{-\pi Msin\omega t}^{\pi Msin\omega t} i_R e^{j(m\omega_c t+n\omega t)} d\omega_c t \;\; d\omega t \;\; e^{-j(2n\pi/3)} \quad (9)$$

$$i_1^{mn} = i_{R1}^{mn} + i_{Y1}^{mn} + i_{B1}^{mn} \quad (10)$$

The harmonic components of the DC-link current i_1 are obtained by summing the respective components of i_{R1}, i_{Y1} and i_{B1} as indicated by (10). The harmonic components are calculated using (7) to (10). A MATLAB code is written for the purpose.

IV. Analytical and Experimental Results

The experimental setup consists of an IGBT based 5 kVA inverter. The controller platform is TMS320LF2407A DSP processor. The switching frequency is 1.5 kHz. The load is a three-phase R-L load. The per-phase inductance of the load is 10 mH. The power factor of the load is varied by changing the resistance of a rheostat in all the three phases of the load. The load current is kept constant at 4 A, by varying the DC bus voltage appropriately. The capacitor current is measured using a fluke-1400S probe. The measured capacitor current waveforms at modulation indices *M*=0.9 and *M*=0.5 are presented in Fig.6, Fig.7, Fig.8 and Fig.9. The waveforms are shown at power factors of 0.137 and 0.844 at both modulation indices.

"The analytical and experimental harmonic spectra of the capacitor current waveforms in Fig.6 to Fig.9 are presented in Fig.10 to Fig.17. The analytically determined spectra pertaining to Fig.6, Fig.7, Fig.8 and Fig.9 are shown in Fig.10, Fig.12, Fig.14 and Fig.16 respectively. The respective experimental spectra are given in Fig.11, Fig.13, Fig.15 and Fig.17. The analytical spectra are obtained as detailed in section III. The experimental spectra are obtained by

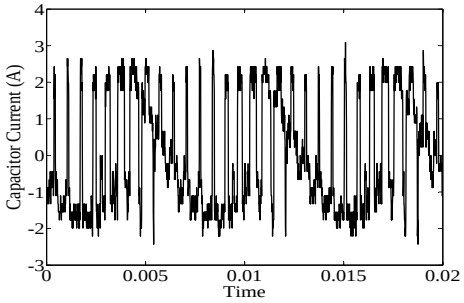

Fig. 7. Capacitor current waveform at I_M=4 A, modulation index of 0.9 at power factor of 0.137

applying Fast Fourier Transform (FFT)on the measured current waveform using MATLAB.

As seen from Fig.10 to Fig.17, the analytical and experimental spectra match reasonably well with each other. Also, the capacitor current contains third harmonic and switching frequency components. The amplitude of the third harmonic component decreases with increase in power factor. On the contrary, the magnitude of the switching-frequency component increases with load power factor. The third harmonic is the only significant low frequency component present in the current spectrum. Hence the voltage ripple in the DC capacitor is determined mainly by the third harmonic component.

V. Evaluation of Power Loss in the DC-Link Capacitor

The power loss in a DC-link capacitor is due to the ripple current flowing through it and ESR of the capacitor. The ESR of the capacitor is dependent on frequency [8]. Equation (11) gives the power loss in a DC-electrolytic capacitor.

$$P = \sum_{n=1}^{\infty} I_{C1}^2(n) ESR(n) \quad (11)$$

Here $I_{C1}(n)$ is the RMS value of n^{th} harmonic of the capacitor current; ESR(n) is the ESR at n^{th} harmonic frequency (i.e. n times the fundamental frequency). The capacitor used is ALCON PG6DI, 450V, 4700uF electrolytic capacitor [9]. The ESR values of the capacitor at different

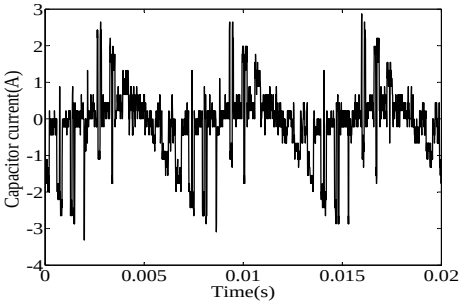

Fig. 8. Capacitor current waveform at I_M=4 A, modulation index of 0.5 at power factor of 0.844

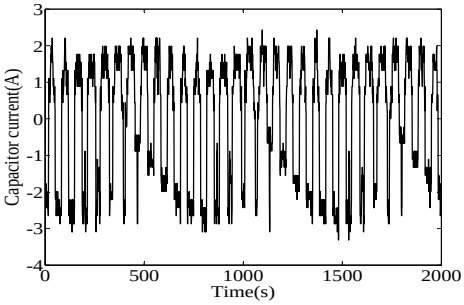

Fig. 9. Capacitor current waveform at I_M=4 A, modulation index of 0.5 at power factor of 0.137

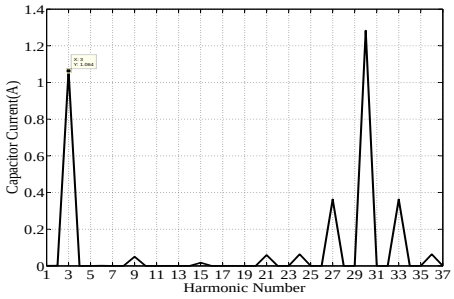

Fig. 10. Analytical harmonic spectrum of DC-capacitor current for I_M=4 A, modulation index of 0.9 and power factor of 0.844

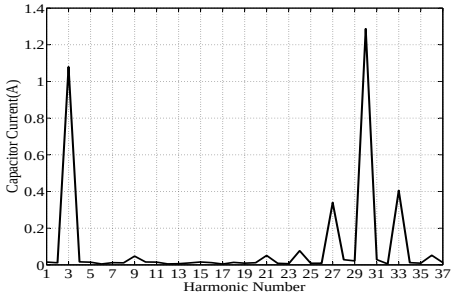

Fig. 11. Experimental harmonic spectrum of DC-capacitor current for I_M=4 A, modulation index of 0.9 and power factor of 0.844

frequencies, as supplied by the manufacturer, are shown in Table II. A curve fit on these data points is done using MATLAB. The resulting equation for the capacitor ESR at a base temperature of $25°C$ is given in (12). A plot of the ESR versus frequency is shown in Fig.18.

$$ESR(n) = \frac{0.0250}{(1 + (0.2025n^2))} + 0.0280 \qquad (12)$$

Using the harmonic spectra evaluated in section III and ESR as given by Fig.18, the power loss in the DC capacitor is evaluated. The power loss is evaluated at the operating conditions corresponding to Fig.10 to Fig.17. These are shown in Table III.

Frequency(Hz)	ESR(ohm)
100	0.0041
150	0.0036
300	0.0032
500	0.0030
5000	0.0028

TABLE II
ESR VALUE AT VARIOUS FREQUENCIES [9]

VI. CONCLUSION

Double Fourier integral and geometric wall model are used to obtain the DC-link capacitor current spectra in a sinusoidally modulated neutral-point clamped inverter. The analytically obtained spectra are validated experimentally. It is shown that the dominant components in the frequency spectra are the third harmonic and switching-frequency components. With a knowledge of the DC-capacitor current harmonic spectrum, the power loss in the DC capacitor is estimated at different operating conditions.

REFERENCES

[1] J. Rodriguez, S. Bernet, P. K. Steimer, and I. E. Lizama, "A survey on neutral-point-clamped inverters," IEEE Trans. Ind. Electron., vol. 57, no. 7, pp. 2219-2230, Jul. 2010.

[2] Kouro, Samir, Mariusz Malinowski, K. Gopakumar, Josep Pou, L. G. Franquelo, Bin Wu, Jose Rodriguez, M. A. Prez, and J. I. Leon, "Recent advances and industrial applications of multilevel converters," IEEE Trans. Ind. Electron., vol. 57, no. 8, pp. 2553-2580, Jul.2010.

[3] D. G. Holmes and T. A. Lipo, "Pulse Width Modulation for Power Converters," IEEE press series on power engineering. Piscataway, NJ: IEEE Press, 2003.

[4] J. F. Moynihan, M. G. Egan, and J. M. D. Murphy, "Theoretical spectra of space-vector-modulated waveforms," IEE Trans. Elec. Power Appl., vol. 145, no. 1, pp. 17-24. January 1998.

[5] B. P. McGrath, and D. G. Holmes, "An analytical technique for the determination of spectral components of multilevel carrier-based PWM methods," IEEE Trans. Ind. Electron. vol. 49, no. 4, pp. 847-857, 2002.

[6] M. H. Bierhoff, F. W. Fuchs, "DC-Link Harmonics of Three-Phase Voltage-Source Converters Influenced by the Pulsewidth-Modulation StrategyAn Analysis," IEEE Trans. Ind. Electron., vol. 55, no. 5, pp.2085-2092, May 2008

[7] G. I. Orfanoudakis, M. A. Yuratich, S. M. Sharkh, "Analysis of dc-link capacitor current in three-level neutral point clamped and cascaded H-bridge inverters," IET Trans. Power. Electron. vol. 6, no. 7, pp.1376-1389, August 2013

[8] F. D. Kieferndorf, M. Forster, T. A. Lipo, "Reduction of DC-bus capacitor ripple current with PAM/PWM converter," IEEE Trans. Ind. Appl., vol. 40, no. 2, pp.607-614, March/April 2004

[9] "Aluminum Electrolytic Capacitors - catalogue no. PG-6DI-00-00". ALCON electronics Pvt Ltd, Jan-2011. URL: www.icd-sales.com.

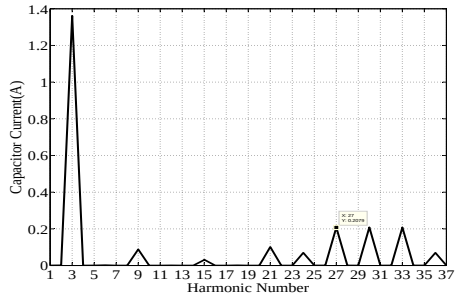

Fig. 12. Analytical harmonic spectrum of DC-capacitor current for I_M=4 A, modulation index of 0.9 and power factor of 0.137

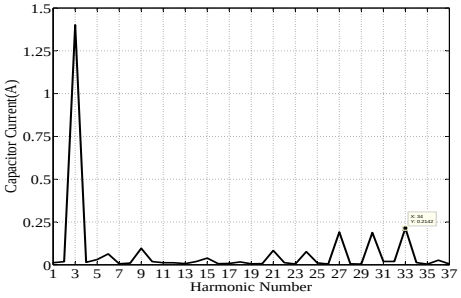

Fig. 13. Experimental harmonic spectrum of DC-capacitor current for I_M=4 A, modulation index of 0.9 and power factor of 0.137

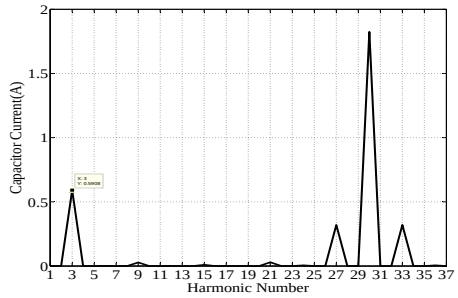

Fig. 14. Analytical harmonic spectrum of DC-capacitor current for I_M=4 A, modulation index of 0.5 and power factor of 0.844

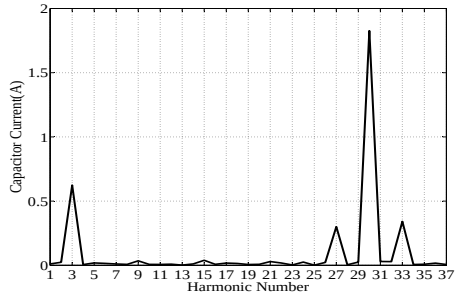

Fig. 15. Experimental harmonic spectrum of DC-capacitor current for I_M=4 A, modulation index of 0.5 and power factor of 0.844

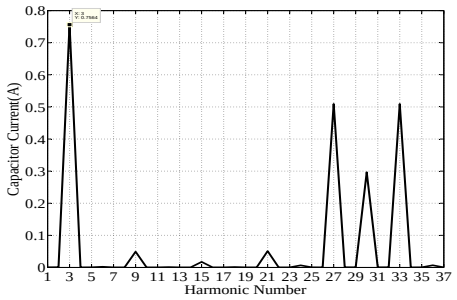

Fig. 16. Analytical harmonic spectrum of DC-capacitor current for I_M=4 A, modulation index of 0.5 and power factor of 0.137

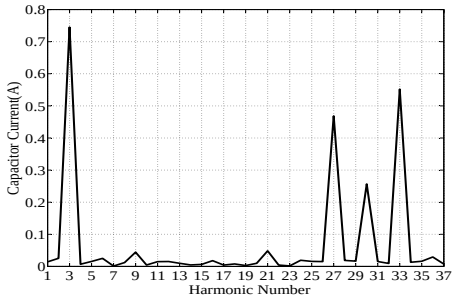

Fig. 17. Experimental harmonic spectrum of DC-capacitor current for I_M=4 A, modulation index of 0.5 and power factor of 0.137

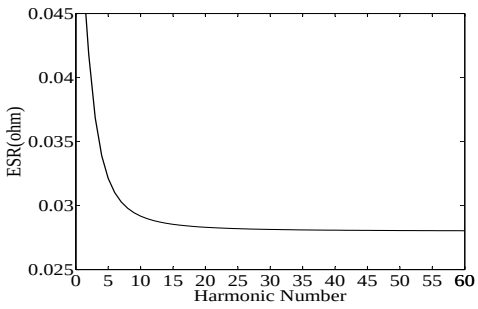

Fig. 18. Plot of ESR versus harmonic number

Modulation index	Load current(A)	Power factor	Power loss(W)
0.9	4	0.844	0.0615
0.9	4	0.137	0.0714
0.5	4	0.844	0.0265
0.5	4	0.137	0.0820

TABLE III
POWER LOSS ESTIMATED AT VARIOUS OPERATING CONDITIONS